

Point-contact spectroscopy in incommensurate chromium

H. Meekes

Research Institute for Materials, University of Nijmegen, Toernooiveld, NL-6525 ED Nijmegen, The Netherlands

(Received 7 March 1988)

The effects of the incommensurate spin-density wave on the current-voltage characteristics in pure chromium are investigated, using point-contact spectroscopy. A simple model is given to account for the changes in the Sharvin current as due to the additional gaps in the density of states for the electrons. The results are compared with experimental data, which show a large increase in the resistivity for voltages smaller than the gap energy.

I. INTRODUCTION

Chromium represents a very special element among metals. This is due to the spin-density wave formed by the conduction electrons below its Néel temperature at $T_N=312$ K. This state is even more interesting because of its nearly antiferromagnetic character. In other words, chromium is incommensurate for temperatures below T_N . The incommensurate spin-density wave has been studied very intensively by neutron-diffraction experiments.¹

Due to the incommensurate nature of the electron spin wave, the density of states of the electrons shows many additional gaps besides the ordinary gaps which are a result of the normal lattice periodicity. These additional gaps are present for $2\mathbf{k}=\pm N\mathbf{Q}+\mathbf{K}$, where $\mathbf{Q}=(2\pi/a)(\alpha,0,0)$ ($\alpha\approx 0.962$ at $T=300$ K), is the incommensurate wave vector, $\mathbf{K}\in\Lambda^*$, a reciprocal-lattice vector, and N is an integer. The size of these gaps is expected to become smaller for higher values of N . This structure results in an increase of the bulk resistivity by 35% when changing from currents parallel to \mathbf{Q} to currents perpendicular to \mathbf{Q} .²

A first-order ($N=1$) gap has been observed by many authors³⁻⁵ in infrared reflectance measurements and was found to have a width of approximately 1000 cm^{-1} or 124 meV. The higher-order gaps are expected to appear for much lower energies.

We decided to find out whether these gaps influence the conductivity by measuring the energy-dependent resistance by means of point-contact spectroscopy. This technique allows for a sensitive detection of nonlinear relations between the current and voltage for energies up to the order of 100 meV.

The paper is organized as follows. In Sec. II, the spin-density wave and its effect on the density of states of the electrons in chromium are described. Section III deals with the basic aspects of point-contact spectroscopy and especially the effect of gaps in the density of states on the current through a point contact. The next section briefly summarizes the experimental techniques used and in Sec. V, the results are discussed. We end with a conclusion.

II. THE STRUCTURE AND DENSITY OF STATES IN CHROMIUM

A. The structure of chromium

Above the Néel temperature, chromium forms a bcc paramagnetic structure. At the phase transition to the incommensurate state (phase AF_1), a spin-density wave (SDW) is formed, with a wave vector $\mathbf{Q}=\alpha\mathbf{a}^*$ and a transverse polarization resulting in an orthorhombic basic symmetry ($Immm$). The coefficient α varies from 0.963 to 0.952 between T_N and 4 K. In this phase, domains are formed with the polarization and \mathbf{Q} vector along the (original) cubic axes. On lowering the temperature, a second phase transition occurs at 122 K to phase AF_2 , where the spin direction is flipped resulting in a longitudinal SDW, forming a tetragonal basic structure ($I4/mmm$). In both phases (AF_1 and AF_2) a small induced longitudinal displacive modulation of the lattice is observed,⁶ with wave vector $2\mathbf{Q}$. The superspace symmetry⁷ of the two incommensurate phases was found to be $G(AF_1)=PImmm(2a00)(\bar{1}11)$ and $G(AF_2)=PI4/mmm(2a00)(1\bar{1}11)$.

B. The origin of the SDW

The origin of the itinerant spin wave seems to lie in the fact that the electron band structure of chromium has electron and hole states in the neighborhood of the Fermi level, which are very comparable as their shapes in \mathbf{k} space are concerned. Loomer⁸ found that the octahedral sheets for the electrons around the $\Gamma(0,0,0)$ point in reciprocal space, though somewhat larger, resemble to a large extent the hole sheets of the $H(1,0,0)$ point in the paramagnetic phase. He pointed out that by a shift over $(0.96,0,0)$ the former coincide (nest) fairly well with the latter. He used this nesting and the coupling between the corresponding states to explain the observed incommensurate SDW. Fedders and Martin⁹ worked out this coupling in a two-band model which indeed predicts a phase transition to a SDW ground state. The interaction between the two states is provided by the Coulomb attraction between the electrons and the holes. The nesting seems to be the best for $(\alpha,\delta,0)$ or $(\alpha,0,\delta)$, where $\delta\neq 0$,

i.e., at points somewhat away from the octahedron vertices.

C. Density of states

Besides the properties of the electron band structure discussed above, one can expect effects on the density of states (DOS) due to the additional wave vector of the crystal. If the SDW would be perfectly antiferromagnetic, the states at $\mathbf{Q}' = (\frac{1}{2}, 0, 0)$ and $-\mathbf{Q}'$ would interact, resulting in a gap halfway into the Brillouin zone, in the direction of \mathbf{Q} . The consequence would be a doubling of the (magnetic) unit cell; the bands being folded back into the new Brillouin zone. In the case of an incommensurate wave, these gaps also open, but now at a general point in the Brillouin zone. Strictly spoken, the resulting crystal has lost its translational symmetry in the [100] direction. This symmetry can, however, be restored, by using the forementioned superspace description. The mixing of states resulting in gaps, happens for wave vectors given by $\mathbf{k} = \pm N\mathbf{Q} \pm \mathbf{K}$, where $\mathbf{K} \in \Lambda^*$ and N integer; the gaps, however, becoming smaller for larger values of N . The resulting band structure shows an infinite number of gaps throughout the energy scale. Such a band structure was studied by de Lange *et al.*¹⁰ in a one-dimensional modulated Kronig-Penney model.

The higher-order gaps become more important when higher harmonics of \mathbf{Q} play a more important role in the modulation. In chromium Pynn *et al.*¹¹ have found second and third harmonics in the SDW. The contribution of the second harmonic increases with decreasing temperature, while that of the third harmonic starts to saturate at 220 K. Hence, effects due to the higher-order gaps can be expected to become more appreciable for low temperatures.

III. POINT-CONTACT SPECTROSCOPY

Point-contact spectroscopy (PCS) is a technique which has been proven to be very useful for studying the effects of excitations and their scattering processes with electrons.¹² For this purpose a very sharp point of one metal (or alloy) is brought into contact with another metal and the first or second derivative of the current through the contact with respect to the voltage across the contact is measured as a function of that voltage. The linear contact dimension is assumed to be small compared to the mean free path of the electrons. Therefore the transport through the contact is ballistic. Typical contact resistances are 0.1–10 Ω and voltages are 0–50 mV. For normal metals a constant density of states for the electrons can be assumed if one takes into account that the energies corresponding to the applied voltages are much smaller than the Fermi energy. If electron phonon scattering is dominant, the resulting spectra show an increase of resistance with voltage due to the back flow of electrons through the orifice being scattered by acoustical phonons. The resistance shows large increases when the phonon density of states has a singularity, for instance, for energies of states at the Brillouin-zone boundary (Debye energy).

In our case, the technique is used to observe gaps in the

electron density of states. The singular effects of phonons can be neglected as long as we stay far away from the Debye energy, which is for chromium 38 meV for the longitudinal-acoustical phonons and approximately 32 meV for the transverse-acoustical phonons.¹³ We implicitly exclude effects due to gaps in the phonon density of states which result from a small induced modulation of the lattice characterized by a wave vector $\mathbf{k} = 2\mathbf{Q}$. A comparable use of PCS has been made by Moser *et al.*¹⁴ to observe anomalies in the electron DOS in CePd₃ and related compounds. For our purpose it is sufficient to concentrate on the first-order derivative $\partial V/\partial I$ as a function of the voltage V .

We will illustrate the effect of the SDW on the $\partial V/\partial I$ spectrum in chromium by assuming that the electron band properties of the basic structure (no modulation) resemble those of the free-electron gas. The effects of the additional wave vector of the SDW as given by \mathbf{Q} is to open gaps whenever two surfaces of constant energy in \mathbf{k} space (spheres in our approximation) at $\mathbf{k} = \pm\mathbf{Q} \pm \mathbf{K}$, where $\mathbf{K} \in \Lambda^*$ cross each other. This can be understood if we use the full symmetry of the crystal as provided by the superspace description, where the reciprocal-lattice vectors are labeled by four integers (h, k, l, m) . This four-dimensional vector corresponds in three dimensions to the vector $h\mathbf{a}^* + k\mathbf{b}^* + l\mathbf{c}^* + m\mathbf{Q}$. As the basic reciprocal-lattice vectors ($m=0$) are concerned, we can neglect the effect of the energy shift on the Fermi level, due to the voltage across the contact; the Fermi level is raised but the metal-like band structure is considered to be constant for the voltages applied. The wave vector \mathbf{Q} , however, provides for gaps in the neighborhood of or even centered on the Fermi level. Therefore, these gaps can be crossed by applying relatively small voltages. Moreover, as will be shown hereafter, all additional gaps below the Fermi level contribute to the increment of the resistance. The above-mentioned illustration will therefore be given for free-electron energy levels, whose spheres do not touch the Brillouin-zone boundary of the basic structure ($m=0$), but do cross the corresponding boundary in superspace. This is possible because h and m can be chosen as to result in a very small wave vector as compared to, say, $(1, 0, 0) \in \Lambda_3^*$. The crossing of the energy bands results in orbits that open and close as a function of the energy, as can be seen schematically in Fig. 1. The directions in \mathbf{k} space, perpendicular to \mathbf{Q} , are in our approximation independent of the modulation. Therefore, one can use, for example, the results of the one-dimensional Kronig-Penney model of de Lange *et al.*¹⁰ for the band structure along the direction of \mathbf{Q} .

The contributions of the forementioned orbits to the current through the contact is calculated as follows. Because the linear dimensions (b) of the orifice of the contact are small compared to the mean free path (l) of the electrons, $b \ll l$, the corresponding, so-called Sharvin current through the orifice is determined by the ballistic transport of electrons from the metal with the higher (V) potential, to the other metal:

$$J_{\text{Sh}} = \frac{2e}{(2\pi)^3} \int_{\text{orifice}} d^2r \int d^3k v_n f^0(\mathbf{r}, \mathbf{k}), \quad (1)$$

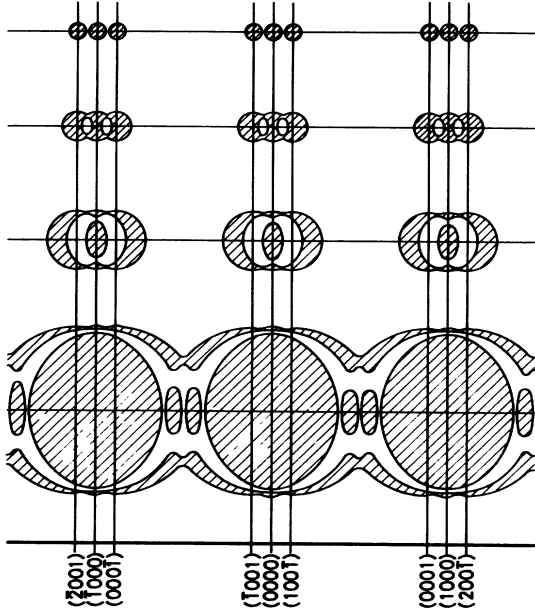


FIG. 1. Schematic drawing of open and closed orbits on surfaces of constant energy for four different values. Each surface is drawn as a projection from four-dimensional superspace in the $(\mathbf{a}^*, \mathbf{b}^*)$ plane in an extended zone scheme. Note that the directions along \mathbf{b}^* and \mathbf{c}^* are free-electron-like. The lattice vectors in reciprocal space are denoted by (h, k, l, m) . For the sake of clarity only the first-order gaps are given. Shaded areas represent occupied surfaces. Each of the four energies lies in a different band within the conduction band.

where v_n is the component 0 of the electron velocity perpendicular to the orifice, f^0 is the electron distribution function, and e is the electron charge. The integration in \mathbf{k} space involves all \mathbf{k} vectors that can contribute to the current, for which v_n is positive and the corresponding energy lies between ε_F and $\varepsilon_F + eV$. These restrictions are denoted as a prime at the integral. At zero temperature this can be written as

$$J_{\text{Sh}} = \frac{2e}{(2\pi)^3} (\pi b^2) \frac{1}{\hbar} \int' d^3k \frac{\partial \varepsilon(\mathbf{k})}{\partial k_n}, \quad (2)$$

where we have assumed a circular orifice with radius b . $\varepsilon(\mathbf{k})$ is the energy of the electron. For the unperturbed free-electron gas (FEG) we have $\varepsilon(\mathbf{k}) = \hbar^2 k^2 / 2m$, thus finding

$$J_{\text{Sh}}^{\text{FEG}} = \frac{2e}{(2\pi)^3} (\pi b^2) \frac{2\pi m}{\hbar^3} \varepsilon_F \int_{\varepsilon_F}^{\varepsilon_F + eV} d\varepsilon = \frac{e^2 b^2}{2\pi} \frac{m}{\hbar^3} \varepsilon_F V, \quad (3)$$

if we assume for the Fermi energy that $\varepsilon_F \gg eV$. (For normal metals $eV/\varepsilon_F \approx 10^{-3} - 10^{-4}$.) The resistance is therefore independent of the energy of the electrons, resulting in a linear relation between the current and voltage. When we introduce the modulation to the problem, the factor ε in the integrand of (2) in general is no longer a continuous function of k_n , due to the additional gaps in the spectrum (cf. the normal energy bands in a crystal field). Thus Eq. (2) becomes

$$J_{\text{Sh}} = \frac{2e}{(2\pi)^3} (\pi b^2) \frac{1}{\hbar} \sum_s \int' d^3k \frac{\partial \varepsilon_s(\mathbf{k})}{\partial k_n}. \quad (4)$$

If we replace the integral in \mathbf{k} space by an integral over the energy, we find

$$J_{\text{Sh}} = \frac{2e}{(2\pi)^3} (\pi b^2) \frac{1}{\hbar^2} \sum_s \int d\varepsilon_s \int dS_{\mathbf{k}} \mathbf{n}_{\mathbf{k}} \cdot \mathbf{s}_{\mathbf{k}}, \quad (5)$$

where $\mathbf{n}_{\mathbf{k}}$ is a unit vector in the direction of the velocity of the electron and $\mathbf{s}_{\mathbf{k}}$ is a unit vector perpendicular to the orifice. $S_{\mathbf{k}}$ is a surface of constant energy in \mathbf{k} space. From (5) we conclude that for every energy ε_s the projection of the corresponding surface in \mathbf{k} space on the plane of the contact determines the Sharvin current. We will distinguish between two different cases for which the orifice normal is either parallel or perpendicular to \mathbf{Q} . In the former case we need the projection along k_x , while in the latter situation the projection along k_z (or k_y) should be used. Fig. 1 can be an aid for a visualization. As the exact band structure of chromium is too complicated, we will continue our simplification by splitting the energy in a part that depends on \mathbf{k} vectors perpendicular to \mathbf{Q} and one depending on \mathbf{k} vectors parallel to \mathbf{Q} :

$$\varepsilon(\mathbf{k}) = \varepsilon_{\perp}(k_y, k_z) + \varepsilon_{\parallel}(k_x), \quad (6)$$

where $\varepsilon_{\perp} = (\hbar^2/2m)(k_y^2 + k_z^2)$ and $\varepsilon_{\parallel}(k_x)$ depends on the actual modulation amplitude. Then Eq. (4) reduces to

$$J_{\text{Sh}}^{\parallel} = \frac{2e}{(2\pi)^2} \frac{(\pi b^2)}{\hbar^3} \sum_s \int_{\varepsilon = \varepsilon_{\perp} + \varepsilon_{\parallel}} d\varepsilon_{\perp} \int d\varepsilon_{\parallel s}. \quad (7)$$

The summation over s involves all bands between $\varepsilon = \varepsilon_F$ and $\varepsilon = \varepsilon_F + eV$. In Fig. 2 the area relevant for the integrals is shaded. Using this figure and slightly overestimating the small triangular contribution of the highest occupied band, we find

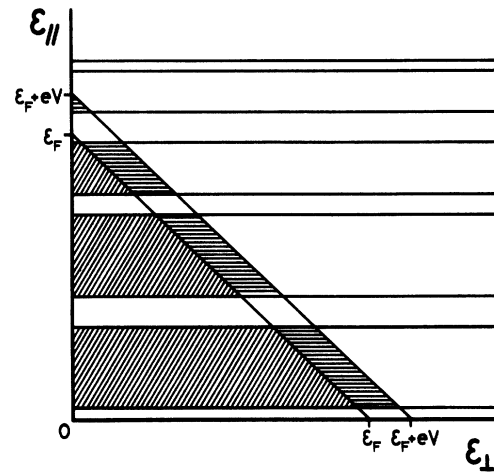


FIG. 2. Schematic drawing of the surface of constant energy as a function of the applied voltage in energy space. Note that $\varepsilon = \varepsilon_{\perp} + \varepsilon_{\parallel}$. For directions parallel to \mathbf{Q} the energy bands (shaded areas indicate filled bands) are present, while in the perpendicular direction the electrons are assumed to be free.

$$J_{\text{Sh}}^{\parallel} = \frac{e^2 b^2}{2\pi} \frac{m}{\hbar^3} V \sum_s \int d\varepsilon_{\parallel s}. \quad (8)$$

Analogously, we find for the current when the orifice normal (say \mathbf{z}) is perpendicular to \mathbf{Q} :

$$J_{\text{Sh}}^{\perp} = \frac{e^2 b^2}{2\pi} \frac{1}{\pi \hbar} \left(\frac{2m}{\hbar^2} \varepsilon_F \right)^{1/2} V \sum_s \int dk_{xs}, \quad (9)$$

where we have used $\varepsilon_z = \hbar^2 k_z^2 / 2m$. From the last two equations we conclude that whenever $\varepsilon(V)$ crosses a gap, the Sharvin resistance stays constant. Between two gaps the conductivity increases linearly for a contact with its normal parallel to \mathbf{Q} , while for the case perpendicular to \mathbf{Q} , the band structure at the edges determines the conductivity. This result is schematically drawn in Fig. 3. An important result is that the structure due to the gaps in the $\partial V / \partial I$ spectra is roughly the same for all orientations of the point contact.

Up to now only the gaps at $\mathbf{k} = \pm N\mathbf{Q} \pm \mathbf{K}$ with $N = 1$ have been considered. Higher harmonics of \mathbf{Q} can (and in chromium do¹¹) play a role, the corresponding gaps being smaller. The effects of these higher-order gaps on the Sharvin resistance is analogous to what was described for the first-order gaps. At this point it is worthwhile to make an estimation of the size of the change in the Sharvin current due to these gaps. An essential difference between chromium and a normal metal is the contribution of all gaps between occupied bands s (see Fig. 2) decreasing the current in chromium. The Fermi energy in antiferromagnetic chromium is approximately 7 eV according to the band-structure calculations of Asano and Yamashita.¹⁵ The first-order gap in the neighborhood of the Fermi level is of the order of 100 meV. Therefore, this single gap already causes a 1.4% decrease of the current for contact normals parallel to \mathbf{Q} , at least in our model. If we also take into account the effect of the other

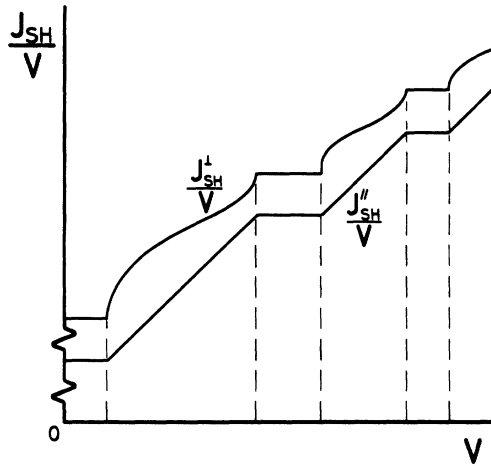


FIG. 3. The Sharvin conductivity, schematically, as a function of the applied voltage for point-contacts parallel and perpendicular to \mathbf{Q} . The constant regions in $J_{\text{Sh}}^{\parallel}/V$ represent the gaps. It should be noted that for normal applied voltages only one gap is traversed.

gaps in the conduction band (see de Lange and Janssen¹⁰) we can expect larger decreases of the current.

IV. EXPERIMENT

A single crystal of chromium was obtained from a Czochralski growth. The resulting crystal ($\approx 7 \times 7 \times 4 \text{ mm}^3$) was oriented by means of x rays and spark cut to obtain specimens with faces perpendicular to the cubic axes. The crystals were then etched electrochemically. At first, point contacts were made between these samples using the Kharkow configuration, for which two fairly sharp edges of the samples are gently pressed against each other. In later experiments these samples were forced to single- \mathbf{Q} domains by applying a magnetic field of 8 T above the Néel temperature and thus slowly cooling down (0.5–1 K/min) to room temperature. Afterwards they were immediately cooled down to 4.2 K in a He-bath cryostat. A third series of measurements was performed by placing a sharp etched tungsten needle on a chromium bulk sample which was also magnetically oriented as described above. All measurements were performed at 4.2 K or lower, down to 1.2 K. First derivatives $\partial V / \partial I$ versus V were measured with a four contact configuration in a compensating resistance bridge, using lock-in techniques.

V. RESULTS AND DISCUSSION

All measurements showed an anomalous behavior around zero-bias voltage. For normal pure metals, the first derivative $\partial V / \partial I$ shows a minimum for zero-bias voltage. The signal becomes bigger for higher voltage mainly due to electrons which, after being scattered by phonons, reenter the orifice, thus increasing the resistance. A comparable behavior is observed in chromium, although a broad symmetric peak around zero indicates an additional increase of the resistivity for low voltages. The shape and height of this anomaly differs for different point contacts. In Fig. 4 some shapes are given for several point contacts. As can be seen in this figure, the fraction of the differential resistance of the anomaly, as compared to the zero-bias point-contact resistance, varies from approximately 3% to more than 25%. The voltage for which an increasing resistivity becomes the main feature varies from 20 mV to approximately 100 mV, with a tendency for high-resistance point contacts to start increasing at higher voltages. In order to find out whether this zero-bias anomaly depends on the orientation of the modulation wave vector with respect to the current through the contact, we measured the spectrum for samples which were oriented in a magnetic field of 8 T, either with \mathbf{Q} parallel or with \mathbf{Q} perpendicular to the point contact. Experimentally there was no significant difference in spectra between these two conditions. This result did not change for a similar experiment using a tungsten spear on a chromium bulk sample. The latter configuration is expected to provide a more reliable orientation of the point contact with respect to the crystal. Once a sample was magnetized, several point contacts with the same orientation of the crystals generally showed comparable peak shapes and heights.

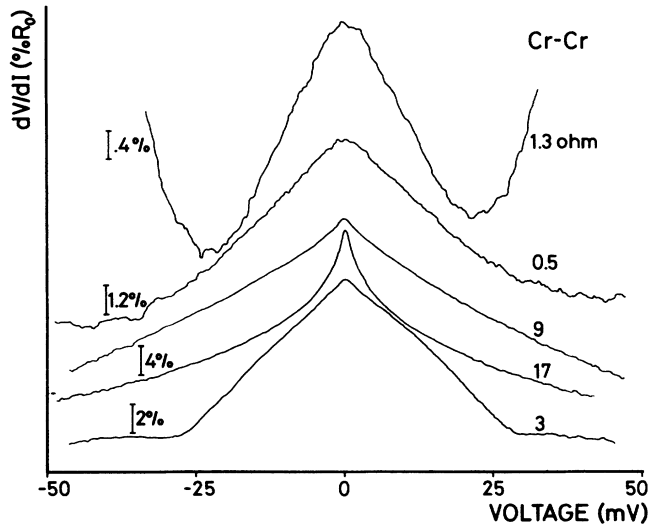


FIG. 4. Some typical point-contact spectra for different Cr-Cr point contacts. The percentages indicate the vertical scale with respect to the zero-bias resistance.

For point contacts, which allowed for high-resistance contacts, it was possible to measure the resistance dependence of the anomaly height. A result of such a measurement is given in Fig. 5. This figure shows that the height of the anomaly is independent of the point-contact resistance over more than one decade, and moreover, that the shape does not change for one and the same point contact. From this result we can conclude that the size of the effect is linear in the contact resistance.

There was no observable temperature dependence of the anomaly between 4.2 and 1.2 K.

Any dependence of the spectrum on magnetic field was not observable up to 15 T, neither for fields parallel to \mathbf{Q} nor for perpendicular fields. The measurements using the tungsten spear turned out to be very sensitive to high magnetic fields, for which the noise increased drastically. This latter effect is probably due to magnetomechanical

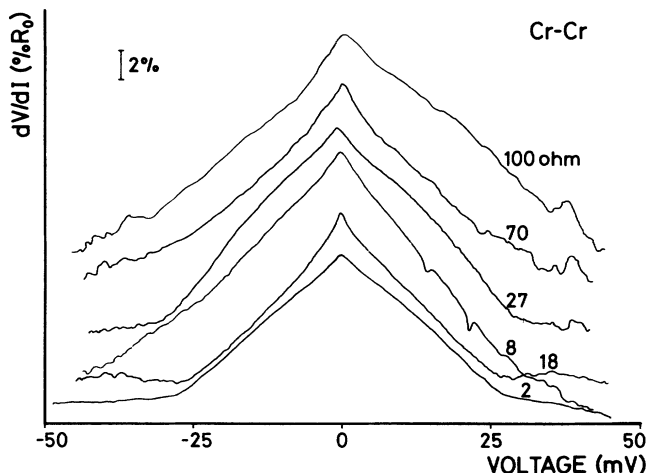


FIG. 5. The zero-bias anomaly for one and the same point contact but different zero-bias resistances.

effects.

Before explaining the observed zero-bias anomaly in terms of gaps in the density of states for the electrons, changing the Sharvin current through the contact, we first will exclude an explanation in terms of heating effects. Heating is known to be often the cause of observed structure in point-contact spectra.¹⁶ The first derivative $\partial V/\partial I$ as a function of voltage then more or less resembles the bulk resistivity as a function of temperature $\rho(T)$. The link between temperature and voltage is achieved by Joule-heating effects, which have only appreciable contributions in the so-called dirty limit (thermal regime), for which both the mean free path of the electrons and the inelastic diffusion length are smaller than the linear contact dimension. These thermal effects can be disregarded in chromium for two reasons. First of all, the dirty limit is in pure metals normally met for high (> 100 meV) voltages and secondly, the resistivity in chromium shows a normal metallike (decreasing) behavior at low temperatures, albeit that the antiferromagnetic part of the resistivity increases with decreasing temperature.¹⁷ Our results for low voltages, when interpreted as due to thermal effects, would suggest an increase of the resistivity at low temperatures. Therefore, heating effects can be disregarded.

As explanation based on the electronic density of states near the Fermi level is, given the results of Sec. III, appealing. The actual form of this function, however, is not very well known, surely if one takes into account the influence of the modulation wave. Some remarks, though, can be made. First of all, the height of the anomaly is at most approximately 25% of the zero-bias resistance. For a triangular shape this means a 13% drop in the resistance. This is ten times as large as the value expected due to the single first-order gap and is a measure for the effect of all additional gaps. Moreover, the possibility of obtaining such high resistances as 100Ω with a stable contact indicates also the intrinsic properties of chromium as compared to normal pure metals.

The sizes of the different gaps are too small to be predicted by band-structure calculations. Experimental techniques as x-ray photoemission spectroscopy (XPS) and soft x-ray absorption, used to reveal the band structure, are not adequate for determining the low-energy effects which are relevant here. However, experiments sensitive in the low-energy regime of the conduction electrons have been performed. These are infrared reflectance and inelastic neutron scattering measurements. The values for the energy gap reported by several authors varies considerably. We will first give an overview of the results reported and afterwards compare them with our measurements.

As the infrared reflectance experiments are concerned, Barker and Ditzenberger³ found an energy gap of 1000 cm^{-1} (124 meV) at 80 K. The same value was found by Lind and Stanford⁴ (30 K). These latter authors found an additional peak at 0.45 eV, which disappeared above T_N . Kirillova and Nomerovannaya⁵ found a value of 0.112 eV at 100 K. For all these measurements, the low-energy side of the spectrum was limited to approximately 60 meV. Inelastic neutron scattering experiments range to

lower energy transfers. Using this technique, Ziebeck and Booth¹⁸ found a gap of 16.9 meV at 295 K. They used energy transfers up to 74 meV. The extrapolated value at 0 K, using a BCS-like temperature dependence of the gap, then yields 71 meV. This result is in agreement with that obtained by Moyer *et al.*¹⁹ who fitted magnetic susceptibility data to a theoretical model, thus finding 28 meV for the gap. Barker and Ditzenberger suggest that their result of 124 meV is a measure of the first-order gap due to the SDW. Higher-order gaps are expected to lie at lower energies. An important question for the interpretation of our results is which gaps enclose the Fermi level. For infrared reflectance measurements the effect of a gap, enclosed by or above the Fermi level, is seen as an absorption of radiation for energies higher than the gap, irrespective of its exact position. The only restrictions imposed are that the transition between the bands obeys momentum conservation and that the corresponding transition matrix element is not zero. In an incommensurate structure the equivalence between states at $\mathbf{k}=0$ and $\mathbf{k}=\pm N\mathbf{Q}$ (N integer), allows for transitions from \mathbf{k} to $\mathbf{k}\pm N\mathbf{Q}\pm\mathbf{K}$. This additional transition scheme was used by Lind and Stanford to account for the absorption peak at 0.45 eV. In their explanation, both gaps (0.124 and 0.45 meV) are first-order gaps corresponding to wave vectors \mathbf{Q} and $2\mathbf{a}^*-\mathbf{Q}$, respectively. They used band-structure calculations of Asano and Yamashita,¹⁵ who also discussed the gap structure. The Fermi level lies in the low-energy first-order gap. Addition of small amounts ($<1\%$) of Mn increases the value of \mathbf{Q} . The effect on the reflectivity is to decrease the 0.1 eV absorption peak and increasing the peak at 0.4 eV. For higher percentages Mn, the SDW becomes commensurate and the two first-order gaps merge to one gap at approximately 0.4 eV, as discussed by Bos and Lynch.²⁰ Second-order gaps in the neighborhood of the Fermi level are expected to occur on both sides of the first-order gaps for a metal-like band and small first-order gaps. On the other hand, it is possible that the second-order gap lies inside the first-order gap for a large enough value of the latter gap, resulting in an open orbit within the first-order gap. In this latter case it is possible to find gaps at lower energies than that of the first-order gap. This can account for the lower extrapolated value of 71 meV found by Ziebeck and Booth, although these authors interpret their result in terms of the first-order gap.

As the aim of our measurements was to find gaps at lower energies (see Fig. 4), we also measured the far-infrared reflectivity of our crystal in a nonsingle \mathbf{Q} state in the energy range 6.2–37 meV at room temperature and at 30 K. We found no structure at all, probably because the instrument limited the sensitivity to approximately 1%. For comparison, the first-order gap at 124 meV generally causes a dip of 3% in the reflectivity.³ Our instrumental resolution probably is too small to observe second-order gaps because the corresponding transition probabilities are expected to be considerably smaller. A transition is allowed in principle at least.

As the insensitivity of the anomaly to the direction of the point contact with respect to the modulation wave vector is concerned, we have to distinguish between two

possibilities. The first one is a direct consequence of the results of Sec. III. As already discussed, the difference in spectra for parallel and perpendicular currents is only due to the structure in the density of states near the band edges corresponding to the additional gaps (see Fig. 3). The other possible reason stems from the polarized reflectance measurements of Barker and Ditzenberger.³ These authors used single \mathbf{Q} -state crystals (oriented in 2.5 T, resulting in 10–20% higher bulk conductivity for directions perpendicular to \mathbf{Q}) and found no difference in reflectivity for polarizations parallel or perpendicular to \mathbf{Q} . They conclude that, given the infrared skin depth, the modulation wave vector in at least the first 200 Å near the surface lies in the surface. A magnetic field of 2.5 T would not be strong enough to change the direction of \mathbf{Q} near the surface, due to the intrinsic defect of any surface, pinning the modulation wave. Although their conclusion is not unambiguous, the results clearly show a preference for the wave vector to have a fixed orientation with respect to the surface. Therefore, the point-contact spectra, which measure the effect of the modulation over a distance of the mean free path of the electrons from the surface, are expected to show no appreciable dependence on the bulk orientation of \mathbf{Q} . Whether, despite the magnetic alignment procedure, our measurements involve only contact normals parallel or perpendicular to \mathbf{Q} is still an open question for us. Moreover, misalignment of the point contact with respect to the surface normal can also account for differences in spectra of several contacts. And as was mentioned before, the first reason mentioned above, namely, the results (8) and (9) of Sec. III, suggest already a small difference for currents parallel or perpendicular to \mathbf{Q} .

This brings us to the question why the zero-bias anomaly manifests its minimum at different voltages for different contacts. To answer this question we have to distinguish between three different contributions to the Sharvin resistance of the contact: the gap structure in the density of states, the scattering by phonons, and Joule heating. The first reason has already been discussed in detail.

The increase of the resistance for higher voltages due to scattering by phonons normally is of the order of a few percent of the zero-bias resistance and is limited by the Debye energy. The increase of the resistance in our measurements, however, always continues up to voltages well above the Debye energy (32 meV for the transverse-acoustical phonons, which provide the main contribution to the scattering process). Furthermore, the increment in resistance is often far too big to be accounted for by phonon scattering only.

Heating effects, on the other hand, are more probable. As mentioned before, such effects normally occur in pure metals for voltages of the order of 100 meV. The size of the effect is expected to increase with decreasing point-contact resistance. This actually is what we on the average observe. Typical low-resistance point contacts ($R_0 \leq 1 \Omega$) have spectra that increase already at 20–40 meV, while contacts with a relatively large resistance ($R_0 \geq 5 \Omega$) have a zero-bias anomaly continuing up to maximal 100 meV. This latter category of contacts either

shows an increase of resistance for higher voltages or even tends to saturate (see, e.g., the 3- Ω spectrum in Fig. 4). There are a few exceptions to this behavior (see, e.g., the 0.5- Ω spectrum in Fig. 4, which does not increase until approximately 40 meV) but this abnormal behavior can be attributed to the actual point contact with all its unknown incidental peculiarities. In any way, the increasing resistance seemingly depends more on the point contact itself, rather than on the structure of chromium.

The fact that for energies still inside the gap, the Sharvin current increases with increasing voltage, indicates that our model is too crude to predict the exact shape of the spectra. In particular, the assumption that the dispersion relations in mutually perpendicular directions are independent of each other appears to be nonrealistic. We expect for the gaps a k_y and k_z dependence too, which, moreover, diminishes on approaching the gap edges. This can account for the decreasing resistance for increasing applied voltage.

VI. CONCLUSION

In conclusion, we can say that in our Cr-Cr point-contact spectra, the zero-bias anomaly is a measure for the gaps in the density of states due to the modulation wave, which, depending on the point-contact resistance, is diminished by heating effects, causing an increase of the resistance. The origin of the anomaly is probably mainly due to the first-order gap because the maximal voltage for which the anomaly is observed is approximately 100 meV in fair agreement with the results ob-

tained by infrared spectroscopy and inelastic neutron scattering. The actual forms of the anomaly, triangle shaped, rounded, or even with a sharp cusp at zero-bias voltage, probably depends on the orientation of the point contact with respect to the surface of the crystal (and correspondingly to the modulation wave vector Q). The effect of gaps lying at lower energies is intrinsically present, because the effect of the single first-order gap is relatively big compared to the zero-bias resistance, which can become unusually high in the case of chromium. The actual shape of the anomaly cannot be fully explained within our simple model. A more realistic approach for which, e.g., the dependence of the gap structure on k_y and k_z is also taken into account is required. The results as given in Fig. 5, where heating effects are not yet dominant, indicate that the height of the anomaly depends linearly on the resistance. This is in agreement with (8) and (9), the Sharvin resistance being inversely proportional to the area of the point-contact orifice.

ACKNOWLEDGMENTS

We gratefully acknowledge Professor R. Griessen, who provided the single crystal, the stimulating discussions with Dr. A. P. van Gelder, and critical reading of the manuscript by Professor A.G.M. Zanner. This work is part of the research program of the Stichting voor Fundamenteel Onderzoek der Materie (Foundation for Fundamental Research on Matter) and was made possible by financial support from the Nederlandse Organisatie voor Zuiver-Wetenschappelijk Onderzoek (Netherlands Organization for the Advancement of Pure Research).

¹For a review, see A. Arrott and S. A. Werner, in *Magnetic and Inelastic Scattering of Neutrons*, edited by T. J. Rowland and P. A. Beck (Gordon and Breach, New York, 1968).

²A. J. Arko, J. A. Marcus, and W. A. Reed, *Phys. Lett.* **23**, 617 (1966).

³A. S. Barker and J. A. Ditzenberger, *Phys. Rev. B* **1**, 4378 (1970).

⁴M. A. Lind and J. L. Stanford, *Phys. Lett.* **39A**, 5 (1972).

⁵N. M. Kirillova and L. V. Nomerovannaya, *Fiz. Met. Metalloved.* **40**, 983 (1975).

⁶Y. Tsunoda, M. Mori, N. Kunitomi, Y. Teraoka, and J. Kanamori, *Solid State Commun.* **14**, 287 (1974).

⁷A. Janner and T. Janssen, *Acta. Cryst. A* **36**, 399 (1980).

⁸W. M. Lomer, *Proc. Phys. Soc.* **80**, 489 (1962).

⁹P. A. Fedders and P. C. Martin, *Phys. Rev.* **143**, 245 (1966).

¹⁰C. de Lange and T. Janssen, *Phys. Rev. B* **28**, 195 (1983).

¹¹R. Pynn, W. Press, S. M. Shapiro, and S. A. Werner, *Phys. Rev. B* **13**, 295 (1976).

¹²A. G. M. Jansen, A. P. van Gelder, and P. Wyder, *J. Phys. C* **13**, 6073 (1980).

¹³W. M. Shaw and L. D. Muhlestein, *Phys. Rev. B* **4**, 969 (1971).

¹⁴M. Moser, F. Hulliger, and P. Wachter, *Physica B + C* **130B**, 21 (1985).

¹⁵S. Asano and J. Yamashita, *J. Phys. Soc. Jpn.* **23**, 714 (1967).

¹⁶I. K. Yanson and O. I. Shklyarevskii, *Fiz. Nizk. Temp.* **12**, 899 (1986) [*Sov. J. Low Temp. Phys.* **12**, 509 (1986)].

¹⁷D. B. Mcwhan and T. M. Rice, *Phys. Rev. Lett.* **19**, 846 (1967).

¹⁸K. R. A. Ziebeck and J. G. Booth, *J. Phys. F* **9**, 2423 (1979).

¹⁹C. A. Moyer, S. Aaraj, and L. Hedman, *Phys. Rev. B* **14**, 1233 (1976).

²⁰W. Bos and D. W. Lynch, *Phys. Rev. B* **2**, 4567 (1970).